The androgen receptor does not directly regulate the transcription of DNA damage response genes.

Sylwia Hasterok[1#], Thomas G. Scott[2#], Devin G. Roller[1], Adam Spencer[1], Arun B. Dutta[2], Kizhakke M Sathyan[3], Daniel E. Frigo[4-7], Michael J. Guertin[3,8], and Daniel Gioeli[1,9]*

[1] Departments of Microbiology, Immunology, and Cancer Biology, University of Virginia, Charlottesville, Virginia, United States of America

[2] Department of Biochemistry and Molecular Genetics, University of Virginia, Charlottesville, Virginia, United States of America

[3] R. D. Berlin Center for Cell Analysis and Modeling, University of Connecticut, Farmington, Connecticut 06030, USA

[4] Department of Cancer Systems Imaging, University of Texas MD Anderson Cancer Center, Houston, TX, USA

[5] Department of Genitourinary Medical Oncology, University of Texas MD Anderson Cancer Center, Houston, TX, USA

[6] Center for Nuclear Receptors and Cell Signaling, University of Houston, Houston, TX, USA

[7] Department of Biology and Biochemistry, University of Houston, Houston, TX, USA

[8] Department of Genetics and Genome Sciences, University of Connecticut, Farmington, Connecticut 06030, USA

[9] Cancer Center Member, University of Virginia, Charlottesville, Virginia, United States of America

[#] These authors contributed equally to the work.

* To whom correspondence should be addressed. Daniel Gioeli, Department of Microbiology, Immunology, and Cancer Biology, University of Virginia, Charlottesville, Virginia, 22908, United States of America. Tel: 434-982-4243; Email: dgg3f@virginia.edu

Abstract

The clinical success of combined androgen deprivation therapy (ADT) and radiation therapy (RT) in prostate cancer (PCa) created interest in understanding the mechanistic links between androgen receptor (AR) signaling and the DNA damage response (DDR). Convergent data have led to a model where AR both regulates, and is regulated by, the DDR. Integral to this model is that the AR regulates the transcription of DDR genes both at steady state and in response to ionizing radiation (IR). In this study, we sought to determine which immediate transcriptional changes are induced by IR in an AR-dependent manner. Using PRO-seq to quantify changes in nascent RNA transcription in response to IR, the AR antagonist enzalutamide, or the combination of the two, we find that enzalutamide treatment significantly decreased expression of canonical AR target genes but had no effect on DDR gene sets in PCa cells. Surprisingly, we also found that the AR is not a primary regulator of DDR genes either in response to IR or at steady state in asynchronously growing PCa cells. Our data indicate that the clinical benefit of ADT and RT is not due to the direct regulation of DDR gene transcription by AR.

Introduction

Prostate cancer (PCa) continues to rank as one of the leading cancers in men worldwide (1). PCa growth and survival are highly dependent on androgen receptor (AR) signaling (2). AR activation is a major driving force behind not only the development and progression of androgen-dependent PCa but also the progression to incurable, lethal, castration-resistant prostate cancer (CRPC) (3). To date, standard of care treatments for advancing PCa range from surgery, chemotherapy, radiation therapy (RT), androgen deprivation therapy (ADT), and combinations thereof (4).

Since there is a demonstrated clinical benefit for combining ADT with RT for PCa, many studies have explored the link between the DNA damage response (DDR) and AR (5,6). There are multiple connections between the AR and the DDR, culminating in a model where the AR both regulates, and is regulated by, the DDR. Key studies a decade ago suggested the model that activation of the AR by ionizing radiation (IR) increases the transcription of DDR genes, leading to rapid repair of DNA damage and promoting radioresistance in PCa cells (7–9). These papers provided evidence that radiation-induced DNA damage enhances the AR-mediated expression of genes involved in DNA damage repair. Additionally, androgens regulate the expression of the catalytic subunit of DNA-PK, a critical component of non-homologous end joining that is responsible for engaging repair factors at sites of DNA damage, promoting the resolution of double-stranded breaks and leading to resistance to IR genotoxicity. These findings were supported by subsequent studies indicating androgen and AR regulation of subsets of DDR genes (10,11). In one study, the specific DNA repair genes regulated by AR were particular to the model system and disease state examined (10).

Other studies have provided evidence that the AR is regulated by DDR components. PARP-1 was recruited to AR binding sites, enhancing AR occupancy and transcriptional function (12). Tandem mass spectroscopy analysis identified Ku70 and Ku80 as direct AR-interacting proteins that positively regulate AR transactivation (13). Furthermore, BRCA1 physically interacted with the DNA-binding domain (DBD) of AR to enhance AR transactivation and induce androgen-mediated cell death through p21 expression (14). In contrast, the association of the ligand binding domain (LBD) of AR with hRad9, a crucial member of the checkpoint Rad family, suppressed AR transactivation by preventing the androgen-induced interaction between the n-terminus and c-terminus of AR (15). Other groups reported non-genomic effects as a result of DDR protein-AR interactions. Mediator of DNA damage checkpoint protein 1 (MDC1), an essential player in the Intra-S phase and G2/M checkpoints, physically associated with full length AR (FL-AR) and the AR splice variant v7 (AR^{V7}) to negatively regulate PCa cell growth and migration (16). Another study showed that increased clonogenic survival following IR was a consequence of DNA-PKc directly complexing with both FL-AR and AR^{V5-7}, with radiation increasing these interactions and enzalutamide blocking the association with FL-AR but not AR^{V5-7} (17). Collectively, these data provide evidence that the AR is integrated into the DDR, interfacing at multiple points, and support an integrated mechanistic model of cooperation between the AR and DDR machinery to explain the clinically observed cooperativity of ADT and RT.

Our own work previously demonstrated a connection between AR and CHK2, a cell cycle checkpoint regulator downstream of DNA damage and replication blockade (18,19). We found that IR is a major driver of the CHK2–AR interaction and that binding of CHK2 to the AR

antagonizes its function leading to AR inactivation. Moreover, alterations in CHK2 activity, caused by gene mutations or loss of expression, are common in PCa and support increased AR activity. We proposed that this, in turn, stimulates the DDR machinery, which repairs IR-induced DNA lesions and promotes PCa cell survival. As part of our study, we tested the impact of the CHK2–AR interaction on the transcription of ten different DDR genes previously defined as part of an AR-associated DNA repair gene signature (8). To our surprise, we detected only a modest induction by IR or androgen treatment in two of the ten DDR genes. This inconsistency aligned with the earlier report indicating that the AR-regulated DDR genes may depend on the model system, experimental conditions, and disease state examined (10). This suggests that the model of AR regulating DDR genes is incomplete and needs further examination. One limitation of the aforementioned studies is that transcripts were generally measured with delayed kinetics (typically one to four days) following treatment with hormone, anti-androgens, or IR. Thus, the androgen-responsive genes identified in these studies could include those that are downstream from primary AR targets. We therefore sought to determine the primary AR transcriptional targets induced by IR to uncover missing mechanistic details for how the AR regulates the DDR.

Results

To determine if AR is activated by DNA damage, we measured IR-induced changes in nascent RNA transcription in asynchronously growing androgen-responsive LNCaP cells. We performed precision nuclear run-on sequencing (PRO-seq) on LNCaP cells grown in whole medium 1 hour after treating with 6 Gray (Gy) of IR or a mock treatment (Figure 1A). Principle component analysis (PCA) revealed that IR treatment was the primary driver of transcript variability (Figure 1B). We observed an immediate transcriptional response to the IR-induced DNA damage, with 218 genes significantly activated and 80 genes significantly repressed at a false discovery rate (FDR) of 0.1 (Figure 1C-D; Supplemental Figure 1A). Using gene set enrichment analysis (GSEA) with the Hallmark Gene Sets (20), we explored which biological processes were over-represented in the IR-induced DNA damage transcriptional response (Figure 1E). At an FDR of 0.05, genes in the P53 Pathway were predominately activated, and genes in the Mitotic Spindle and G2/M Checkpoint gene sets tended to be repressed in response to IR. The Hallmark Androgen Response gene set was not identified at an FDR of 0.05 or when the FDR was relaxed to 0.2, suggesting that AR is not directly activated by IR. To identify candidate sequence-specific transcription factors (TFs) that drive the IR induced DNA damage transcriptional response, we first defined putative regulatory elements (e.g. enhancers and promoters) with dREG (21). We identified putative regulatory elements responsive to IR with DESeq2 (Supplemental Figure 1B). Next, we performed *de novo* motif analysis using MEME (22) within the increasing putative regulatory elements and matched these motifs to the JASPAR database (23), and found only the p53 motif (Figure 1F), consistent with the GSEA. We found no motifs within the decreasing putative regulatory elements. Using FIMO (24) to identify

p53 motif instances genome-wide, we found a significant enrichment (Chi-squared test p-value $< 2.2 \times 10^{-16}$) of p53 motifs in IR-activated putative regulatory elements whereas there was no enrichment of p53 motifs in the IR-repressed putative regulatory elements (Figure 1G). These data indicate that the predominant primary transcriptional response triggered by IR in LNCaP PCa cells is driven by p53, consistent with the canonical p53 DNA damage transcriptional response.

To explicitly identify AR-regulated transcripts among the IR-induced DNA damage primary transcriptional response we pretreated LNCaP PCa cells with 10 μM enzalutamide for 30 minutes prior to 6 Gy IR and then performed PRO-seq following a 1-hour incubation post IR (Figure 2A). The 10 μM dose of enzalutamide maximally inhibited LNCaP PCa cell growth (Figure 2B). For additional controls, we confirmed that AR antagonism with enzalutamide and AR activation with the synthetic androgen R1881 was radiosensitizing and radioprotective, respectively (Figure 2C). In exploring the underlying structure of the PRO-seq data using PCA we again found that the predominant discriminating factor is IR (Figure 2D). PC3 separates the enzalutamide samples from the vehicle samples and accounts for 8% of the variance in the data. Hierarchical clustering of the dynamic genes (Figure 2E) segregates treatment groups first by IR and then by enzalutamide, reinforcing that IR is the major driver of gene expression changes relative to enzalutamide. The volcano plots (Figure 2F) illustrate a robust transcriptional response to IR, comparable to what we observed earlier (Figure 1D). See Supplemental Figure 1 for corresponding MA plots. Enzalutamide treatment significantly decreased expression of 182 genes (FDR 0.05); GSEA reveals that these genes represent canonical AR target genes (Hallmark Androgen Response). We find no Hallmark or Reactome

gene set signature of DNA damage within genes significantly changed by enzalutamide (at FDR 0.05 or 0.2).

To further test if AR is part of the primary transcriptional response to IR induced DNA damage, we explicitly examined the changes in expression of the genes in the Hallmark DNA Repair gene set upon either IR or enzalutamide (Figure 2G). IR significantly activated multiple genes, while enzalutamide treatment did not significantly change expression of any genes in the set. We also explicitly surveyed the PRO-seq data for changes in expression of the DDR genes previously defined as AR regulated (7,8,10) (Supplemental Table 1). We did not find any significant changes in response to enzalutamide in the previously defined 32 direct DDR AR target genes (8), or in DNA-PK (7), and only four of 36 previously defined androgen-regulated DDR genes from LNCaP (10) were significantly changed by enzalutamide. Thus, in asynchronously growing PCa cells the AR does not appear to directly regulate the expression of genes in the DDR, even when cells are exposed to IR DNA damage. Next, we examined the effect of enzalutamide and IR on the expression of genes in the Hallmark Androgen Response gene set (Figure 2H). As expected, enzalutamide treatment had a significant effect on many genes in the set. IR both activated and repressed genes in the Hallmark Androgen Response set, indicating that IR does not broadly activate or inhibit AR at all AR target genes. To test this further, we defined a Primary AR Target gene set from our own PRO-seq data of enzalutamide treated LNCaP cells and examined the effect of IR on the expression of these genes (Figure 2I). As with the genes in the Hallmark Androgen Response gene set, expression of Primary AR Target genes both increase and decrease in response to IR, consistent with TFs other than AR regulating gene expression changes in response to IR. Finally, we assessed the proximity

between the transcription start site (TSS) of each gene regulated by IR or enzalutamide to AR or p53 binding sites, as defined by publicly available Chromatin Immunoprecipitation (ChIP) sequencing peaks (25,26). As expected, enzalutamide-repressed genes tend to be closer to AR binding sites, indicating that these genes are direct targets of AR activation at baseline (Figure 2J). Similarly, IR-activated genes tend to be closer to p53 binding sites, consistent with a mechanism in which p53 activates a substantial proportion of these genes in response to IR (Figure 2K). In contrast, IR-responsive genes are not significantly closer to AR binding sites than IR-unchanged genes are, suggesting that AR is not responsible for the IR-responsive transcriptional changes (Figure 2L) and that TFs other than AR drive changes in gene expression induced by IR. Collectively these data indicate that the AR is not part of a primary IR-induced DNA damage transcriptional response in LNCaP PCa cells, nor is AR a primary regulator of genes in the DDR under normal growth conditions. This is further corroborated by analysis of published GRO-seq data of hormone-stimulated LNCaP and VCaP cells (27,28); neither of these studies of the hormone-induced primary AR transcriptional response identified gene sets associated with the DDR. Furthermore, we previously tested for changes in AR S81 phosphorylation in response to IR and found no change in S81 phosphorylation (19). Since the predominant kinase that phosphorylates S81 is CDK9, part of P-TEFb, and S81 phosphorylation is associated with AR transcriptional activity (29–31), the lack of IR induction of AR S81 phosphorylation is consistent with IR not activating the AR (19).

We tested for any role that AR may play in the transcriptional response to IR-induced DNA damage by identifying groups of genes that are regulated by both enzalutamide and IR. We find 32 genes activated by both enzalutamide and IR (Supplemental Figure 2A), 66 genes

repressed by both enzalutamide and IR (Supplemental Figure 2B), 7 genes activated by enzalutamide and repressed by IR (Supplemental Figure 2C), and 16 genes activated by IR and repressed by enzalutamide (Figure 3E). This last group of 16 genes fits the pattern predicted for genes activated by AR in response to DNA damage. Over-representation analysis (ORA) for Hallmark gene sets indicated that the set of 32 genes activated by both enzalutamide and IR is enriched for cholesterol homeostasis genes, and the set of 66 genes repressed by both enzalutamide and IR are enriched for genes involved in androgen response and for genes downregulated by UV radiation (Supplemental Figure 2D); no gene sets were identified for the 7 genes activated by enzalutamide and repressed by IR. ORA indicated that the set of 16 genes activated by IR and repressed by enzalutamide is enriched for the canonical Hallmark Androgen Response gene set (Supplemental Figure 2D). Further examining this set of genes, we found that alterations of these 16 genes in the TCGA PanCancer Atlas were associated with a poorer progression-free survival (PFS) (Supplemental Figure 2E). Interestingly, two of these 16 genes, TLE1 and WNT7B, were individually associated with a poorer PFS. This suggests that although there is only a small subset of primary AR target genes activated by IR, these genes may contribute to PCa progression.

We next examined RNA polymerase II (Pol II) localization within genes responsive to IR, enzalutamide, or both treatments to determine if IR and AR regulate the same step of the Pol II transcription cycle (e.g. initiation, promoter-proximal pausing, elongation, or termination) (32,33). PRO-seq measures the genome-wide location of transcriptionally engaged Pol II at single-nucleotide resolution (34). This spatial precision allows us to determine Pol II density within the promoter-proximal pause region as well as within the gene body and to calculate a

Pause Index (PI) for each gene using the ratio of these two densities (35). IR treatment leads to an increase in Pol II density in both regions within IR-activated genes (Figure 3A). Calculating the ratio of PI for each of these genes in IR relative to control conditions, we find that IR decreases PI, indicating that IR increases the rate of Pol II pause release (Figure 3B). We find that enzalutamide treatment leads to a decrease in Pol II density in both regions within enzalutamide-repressed genes and an increase in PI (Figure 3C and 3D), indicating that enzalutamide decreases the rate of Pol II pause release. These data would suggest that enzalutamide treatment may prevent the release of promoter-proximally paused Pol II on the 16 genes activated by IR and repressed by enzalutamide. Analysis of the changes in PI for the 16 genes is consistent with this prediction (Figure 3F); enzalutamide treatment increased PI, IR decreased PI, and the combined treatment led to an intermediate change in PI approximating zero.

To explore these IR-activated enzalutamide-repressed genes further, we ranked the genes by the magnitude of enzalutamide inhibition of the IR induction below control levels and selected the top half to examine expression levels between normal and tumor tissue. This subset of eight genes was also associated with a poorer PFS in the TCGA PanCancer Atlas (Supplemental Figure 2F). We used Gene Expression Profiling Interaction Analysis (GEPIA2) analyzing the RNA sequencing expression data from the TCGA and the GTEx projects (36). We find that CAMKK2, ELOVL7, and PMEPA1 expression increases in tumor compared to control (Figure 4A). We dropped TMEM132D from further analysis since mRNA expression is very low in prostate and PCa, and the TMEM132D protein does not seem to be expressed (37). We reasoned that, if AR activation was important in the cell response to IR, then the mRNA levels of

these genes would remain elevated over time. We assessed at 24 hours in LNCaP (Figure 4B), C4-2, 22Rv1, and VCaP cells (Supplemental Figure 3) the mRNA levels of CAMKK2, CDC42EP3, ELOVL7, PMEPA1, PVT1, TLE1, and WNT7B in response to 10 μM enzalutamide, 6 Gy IR, or a 30 minute pretreatment with 10 μM enzalutamide followed by 6 Gy IR. In LNCaP cells at 24 hours, enzalutamide significantly reduced expression of five of the seven genes examined: CAMKK2, CDC42EP3, ELOVL7, PMEPA1, and WNT7B. IR significantly induced expression of ELOVL7, PVT1, and TLE1. The mRNA abundance in the combination of enzalutamide and IR was significantly less than in IR alone for CAMKK2, ELOVL7, and WNT7B. Only ELOVL7 showed the same expression pattern at 1 and 24 hours post IR of a significant induction of expression by IR that is significantly antagonized by enzalutamide (Figure 3E and 4B). The expression patterns in C4-2, 22Rv1, and VCaP cells were appreciably different than in LNCaP cells, with only ELOVL7 and PVT1 in C4-2 and TLE1 in 22Rv1 cells increasing with IR. In C4-2 for CAMKK2 and ELOVL7, and in 22Rv1 for TLE1, the IR induction was antagonized by enzalutamide, consistent with these genes being induced by IR in an AR dependent manner. The difference in response of these genes to IR and AR antagonism in the four PCa cell lines suggests that cell line heterogeneity affects the determination of any set of genes that increases with IR in an AR dependent manner. Since ELOVL7 was the only gene with a significant induction of mRNA expression by IR that was antagonized by enzalutamide at both early (1 hour) and late (24 hour) timepoints in LNCaP and a second PCa cell line (C4-2; Supplemental Figure 3C), we next tested for changes in ELOVL7 protein expression over time in response to the same treatments (Figure 4C). We found no significant changes in protein expression from 15 minutes to 6 hours in response to IR, enzalutamide, or the combination thereof (Figure 4D). This suggests that, although the AR may

activate transcription of a small set of genes in direct response to IR-induced DNA damage, additional cellular controls mitigate downstream effects of that activation, preventing sustained changes in mRNA or protein levels.

Since alterations in these genes are associated with a shorter time of PFS (Supplemental Figure 2F), we next tested the impact of altering expression of these genes on PCa cell growth (Supplemental Figure 4). We selected CAMKK2, ELOVL7, and WNT7B as representatives of this gene set; all three have been implicated in PCa (38–41) and ELOVL7 is the only gene from the subset induced by IR and antagonized by enzalutamide at 1 and 24 hrs. Knockdown of ELOVL7 had a profound effect on cell growth, leading to clearing of cells from the knockdown wells (data not shown). Given the cell death induced by ELOVL7 knockdown it was not a surprise to see that enzalutamide treatment had no additional effect, and hormone treatment did not rescue growth when ELOVL7 was knocked down. The effect of WNT7B knockdown was similar to that of ELOVL7 but the effect was not as great. C4-2 cells had the same CAMKK2 expression pattern in response to enzalutamide and IR as LNCaP. Consistent with CAMKK2's role in metabolic fitness (42), under nutrient-replete conditions, CAMKK2 knockout in C4-2 cells had no effect on *in vitro* growth, or response to enzalutamide or R1881 in our assay. These findings are in contrast to the established role of CAMKK2 in CRPC *in vivo* tumor growth (38), and further indicate that additional stresses are needed to reveal CAMKK2's pro-cancer roles.

We next tested the impact of reduced expression of CAMKK2, ELOVL7, and WNT7B on cell response to IR in the presence and absence of hormone and enzalutamide (Supplemental Figure 5). For ELOVL7, knockdown reduced cell survival to the point that IR had no additional effect on survival and androgen offered no protection from the knockdown of ELOVL7.

Knockdown of WNT7B also reduced cell survival, and IR had little additional effect. In C4-2 cells the protective effect of AR activation is minimal, and while CAMKK2 knockout reduced survival overall, there was no sensitization to IR, and R1881 offered minimal protection. We also tested if knockout or knockdown of CAMKK2, ELOVL7, and WNT7B cooperated with enzalutamide and/or IR to reduce cell viability. Parallel effects with AR activation were observed for all three: ELOVL7 knockdown inhibited survival completely preventing any evaluation of cooperativity with enzalutamide; WNT7B knockdown further reduced survival in response to enzalutamide and at low dose IR; and CAMKK2 knockout did not generate enzalutamide sensitivity in C4-2 cells.

A distinguishing feature of our data in comparison to prior work that has indicated that AR regulates the transcription of DDR genes (7,8,10,11) is that, by measuring nascent transcription shortly after enzalutamide treatment, we isolated the primary effects of AR inhibition. Downstream from these primary effects, AR may indirectly regulate DDR genes by activating the transcription of additional TFs that directly regulate DDR genes. Enzalutamide treatment significantly (adjusted p-value <0.05) repressed 17 TFs (Figure 5A). The most enzalutamide-repressed TF in the Hallmark Androgen Response is ZBTB10. In the TCGA PCa data, ZBTB10 amplification is associated with a lower disease-free survival (Figure 5B), and ZBTB10 expression is higher (p-value < 0.01) in tumor than normal (Figure 5C). In LNCaP and C4-2 cells at 24 hours, there was a significant induction of ZBTB10 expression by IR that was significantly antagonized by enzalutamide (Figure 5D, E). There was no effect of IR or enzalutamide on ZBTB10 expression in 22Rv1 cells. In VCaP cells, enzalutamide inhibited ZBTB10 expression, but expression was not affected by IR. We reasoned that, if AR activation of

ZBTB10 expression mediated downstream activation of the previously reported DDR genes trigged by AR response to IR, then overexpression of ZBTB10 should provide some protection from IR as AR activation does (as shown in Figure 2C). ZBTB10 overexpression (Figure 5H, I) had no effect of LNCaP survival in response to IR or enzalutamide treatment (Figure 5F, G), and androgen was still protective, collectively indicating that ZBTB10 expression is not sufficient to phenocopy the protective effect of androgen.

Discussion

There is compelling clinical evidence for the benefit of ADT in combination with RT (43–47). These clinical observations led to studies testing for interplay between the AR and the DDR (5,6). From these studies, the model that emerged was one of cooperation between the AR and DDR machinery; IR-induced DNA damage increases AR activation and transcription of DDR genes, and the AR is regulated by components of the DDR (5–10,12–16). However, specifics of this molecular model were inconsistent across the biological systems used in these studies, suggesting that aspects of this model of AR regulation of DDR genes were incomplete and in need of further examination. Furthermore, most of the studies leading to the model of AR regulating the DDR examined changes in transcription following treatment with hormone, anti-androgens, or IR after one to four days. Therefore, the transcriptional changes measured could be downstream and secondary from primary AR targets. Also, for the studies examining changes in transcription following hormone treatment, cells were often grown in charcoal-stripped serum containing media for one to three days; subsequent stimulation of these cells with hormone transitions cells from a quiescent state to an active growth state and thus, the transcriptional changes measured days later also encompasses growth associated transcript changes in addition to primary AR targets. We therefore sought to identify the immediate transcriptional changes induced by IR in an AR-dependent manner.

We found, counter to what is accepted in the field, that the AR is not a primary regulator of DDR genes. Using AR-positive androgen-responsive LNCaP PCa cells growing asynchronously in medium with whole serum, we measured transcriptional changes in gene expression using PRO-seq to quantify changes in nascent RNA transcription in response to IR,

enzalutamide, and the combination of the two. Antagonizing the AR with enzalutamide significantly decreased expression of canonical AR target genes but had no effect on DDR gene sets. This observation is consistent with previously published GRO-seq data of hormone stimulated LNCaP and VCaP cells, which did not identify any gene sets associated with the DDR (27,28). Examining individual DDR genes defined by previous studies as AR-regulated (7,8,10), we find only 6 of 75 genes significantly changed in response to enzalutamide. IR both increased and decreased canonical AR target gene transcription, and IR-responsive genes are not significantly closer to AR binding sites than IR-unchanged genes are, collectively indicating that the AR is not responsible for the primary IR-responsive transcriptional changes. When we explicitly test for genes activated by IR and repressed by enzalutamide, the pattern predicted for genes activated by AR in response to DNA damage, we find only 16 genes. None of these 16 genes are part of the Hallmark DNA Repair gene set. Furthermore, these genes do not have a consistent response to IR and enzalutamide across different PCa cell lines. Additionally, we did not observe changes in ELOVL7 protein levels in response to IR and enzalutamide treatment despite a robust, conserved, and persistent change in *ELOVL7* mRNA levels under the same experimental conditions in multiple PCa cell lines. Taken together, our data indicate that AR is not part of a primary IR-induced DNA damage transcriptional response in PCa cells, and AR is not a primary regulator of genes in the DDR under normal growth conditions. Therefore, the clinical benefit of combining ADT with RT is likely not due to AR directly regulating transcription of DDR genes in response to IR-induced DNA damage.

The DDR protein – AR interactions are relatively underexplored and could generate a delayed AR transcriptional response in reaction to IR. We measured nascent transcription

following 90 minutes of enzalutamide treatment (30 minutes enzalutamide alone -/+ 60 minutes IR). Interactions of DDR proteins with the AR could lead to primary AR transcriptional changes with delayed kinetics. In response to IR, gH2AX and 53BP1 foci peaked at 2hrs, and when we examined DNA damage using the comet assay, we found that DNA damage was mostly repaired in PCa cells by 2 hours (18). These kinetics suggest that we should have observed a primary AR transcriptional response to IR under the conditions we used here if AR was regulating expression of genes important for DNA repair through DDR protein – AR interactions. If the AR is a critical regulator of the DDR through steady state regulation of genes in the DDR, then one possibility is that this regulation represents a secondary effect mediated through one or more of the 17 TFs directly regulated by the AR. One of these TFs, ZBTB10, is amplified in 8% of PCa in the TCGA dataset, and in 26% in the East Coast SU2C metastatic CRPC (mCRPC) dataset (48,49). However, overexpression of ZBTB10 alone was not sufficient to replace the protective effect from IR afforded by androgen treatment. Interestingly, we observed MYC downregulation in response to enzalutamide, suggesting MYC transcript levels are directly regulated by AR in LNCaP cells. This is in contrast to what was observed in VCaP cells (27) at 2hrs DHT stimulation, suggesting AR regulation of MYC in PCa may be heterogeneous. VCaP cells express the TMPRSS2-ERG fusion (50) and TMPRSS2-ERG can regulate MYC expression levels (51), raising the possibility that MYC may be coordinately regulated by AR and ERG. Overexpression of MYC, in the context of normal AR expression levels, clearly downregulates AR transcriptional programs through coregulator redistribution and Pol II promoter-proximal pausing (52–54), suggesting a negative feedback loop between AR

and MYC. What is still unknown is how AR and MYC transcriptional programs interact at steady state when the relative endogenous expression levels of both MYC and AR are considered (54).

In this study we also examined Pol II localization to determine the impact of IR and AR inhibition on Pol II initiation and promoter-proximal pausing. Interestingly, enzalutamide treatment led to an increase in promoter-proximally paused Pol II. In earlier studies, we found that CDK9, which associates with cyclin T to form pTEFb (55), phosphorylates AR on Ser81 (30). This phosphorylation is required for optimal AR transcriptional activity and association with chromatin, is the highest stochiometric phosphorylation on the AR, and continues to increase over time with hormone treatment (29,30,56,57). Our observation of enzalutamide treament increasing Pol II promoter-proximal pausing lends further support for the model that AR regulates transcription through a feedforward loop involving mobilization of pTEFb, increasing AR pS81 phosphorylation, and co-regulator recruitment that actively sustains the transcription of AR-regulated genes (58).

The data presented here imply that the clinical benefit of ADT in combination with RT is not due to a direct molecular mechanistic interaction between the AR and DDR. If AR antagonism limits DNA repair through reducing expression of DDR genes, as predicted by the integrated model proposed from previous publications (7,8,10,11), then neoadjuvant ADT should be more effective than adjuvant ADT when combined with RT. However, the opposite seems true, adjuvant ADT is more effective than neoadjuvant ADT in combination with RT (47,59). Thus, we propose that the clinical benefit of ADT and RT is not due to the primary AR regulation of DDR gene transcription. The field needs to consider alternative mechanisms for the clinical benefit of combining ADT with RT. Recent studies have shown that androgen

signaling suppresses T-cell immunity against cancer (60,61) raising the possibility that ADT counteracts this immunosuppression, which may be critical to any abscopal effect induced by RT (62,63). Other possible mechanisms could account for the ADT plus RT benefit, including the straightforward possibility that both treatments independently reduce tumor cell fitness.

Methods

Cell culture. LNCaP (RRID:CVCL_0395) and C4-2 (RRID:CVCL_4782) cells (gifts from Dr. L. W. K. Chung) and C4-2 CAMKK2 knockout cells generated previously (38) were grown in DMEM:F12 (Invitrogen) with 5% non-heat inactivated serum (Gemini) and 1% Insulin-Transferrin-Selenium-Ethanolamine (ITS) (ThermoFisher). CWR22Rv1 (22Rv1) (RRID:CVCL_1045; gift from Dr. Steven Balk) and VCaP (RRID:CVCL_2235; gift from Dr. Kerry Burnstein) were grown in DMEM (Invitrogen) with 5% heat-inactivated serum. Commercial DNA fingerprinting kits (ATCC) verified cell lines and all cell lines were tested for mycoplasm.

Cell treatment for gene expression analysis. To determine which sites are actively transcribed in PCa cells upon IR treatment and to see if these changes depend on the AR, four sets of treatments were established: LNCaP cells were plated into 150 mm tissue-culture dishes at 4.2 x 10^6 cells, grown two days in the whole medium under standard growth conditions (37°C, 5% CO_2) and then 1) DMSO (control) vehicle treated for 90 min; 2) DMSO vehicle treated for 30 min plus 6 Gy IR followed by 60 min incubation; 3) 10 µM Enzalutamide for 90 min; and 4) 10 µM Enzalutamide for 30 min followed by 6 Gy IR and incubated for 60 min. Cells were permeabilized as previously described (34).

PRO-seq. PRO-seq library preparation and analysis were performed as previously described (64–66). In brief, cells were permeabilization according to Mahat et al. (2016) (34). The permeabilized cells were counted, and 50 µL aliquots containing approximately 6-8 x 10^6 cells were snap-frozen in liquid nitrogen and stored at −80°C. PRO-seq libraries were prepared

according to Sathyan et al. (2019) (64), which included a random eight-base unique molecular identifier (UMI) at the 5′ end of the adapter ligated to the 3′ end of the nascent RNA. No size selection was performed to avoid bias against short nascent RNAs. The raw PRO-seq sequencing files can be accessed from the NCBI Gene Expression Omnibus (GEO; https://www.ncbi.nlm.nih.gov/geo/) under accession number GSE_TBD. All analysis details and code are available at https://github.com/TBD.

qPCR. RNA isolation and quantitative real-time PCR (qPCR) were performed as previously described (67,68). RNA concentrations were determined using a NanoDrop 2000 UV-Vis Spectrophotometer (Thermo Scientific). cDNA was synthesized using Sensifast cDNA synthesis kit (Bioline, BIO-65054). Quantitative real-time PCR (qPCR) was performed using iTaq Universal SYBR Green Supermix (Biorad, #1725124). Primer sequences: CAMKK2 F: CGTCTCCATCACGGGTATGC, CAMKK2 R: CACCATAGGAGCCCTTTCCA; CDC42EP3 F: GCATTGGTGATGTTCGGCTC, CDC42EP3 R: GCCCTTCATAGCTAGTGCCA; ELOVL7 F: GTTTGGGAACATTCCATGCCC, ELOVL7 R: ATGATGCACGCAAAGACTGG; PMEPA1 F: CTGGTTCAGAGAAGGCCGAG, PMEPA1 R: GAGGACAGGGAATGAACCCG; PVT1 F: TGGAATGTAAGACCCCGACTCT; PVT1 R: GATGGCTGTATGTGCCAAGGT, TLE1 F; GATCTGGGGATCACGCCTTG, TLE1 R: ACCACTGCTCTACAAAGGACG; WNT7B F: CAAAGTCTGCCAGCAACAGG; WNT7B R: CAGCTTTTATTGGGCCGAGC. The relative standard curve method was used to determine transcriptional fold changes as we have done previously (69–72). RNA starting quantities (SQ) were determined using a standard curve. The SQ mean was then normalized to the reference gene PSMB6.

Western blot analysis. Western blotting performed as previously described (67,68). Antibodies: ELOVL7 (Sigma AV49908; used at 1:1000), ZBTB10 (Bethyl Laboratories A303-257A; used at 1:5000), ERK (Cell Signaling 137F5; used at 1:1000), Ran (BD Biosciences #610340; used at 1:2000), and Tubulin (Cell Signaling #2144; used at 1:1000).

Generation of ZBTB10 overexpressing stable cells. Reverse transduction was done by adding plenti-HA virus or pLenti-ZBTB10-HA virus diluted to an MOI of 25 in DMEM-F12 media containing 5% non-heat inactivated FBS and 1x ITS to a fibronectin (1 μg/ml) coated 6 well plate and then adding LNCaP cells to the well. Two days after the reverse transduction, media was changed and 1 μg/ml puromycin selection was added. Cells were fed with selection media every two days until reaching 80% confluency. The cells were then expanded with continued selection until freeze downs could be made for future propagation and experimentation.

Growth assay. Assay was performed as previously described (18). Briefly, shRNAs targeting ELOVL7 (sh#1 sense: ccggtGTTACTTCTCCAAATTTAAtacctgacccataTTAAATTTGGAGAAGTAACTTTTTg; sh#2 sense: ccggtCCTGGTGGTTTGGAGTCAAATCTCGAGATTTGACTCCAAACCACCAGGTTTTTg), or WNT7B (sh#1 sense: ccggtGCATGAACCTGCATAACAAtacctgacccataTTGTTATGCAGGTTCATGCTTTTTg; sh#2 sense: ccggtGTGGCAGTGCAACTGCAAATTctcgagAATTTGCAGTTGCACTGCCACTTTTTg), or Vector control virus was added to fibronectin-coated (1 μg/ml) 96 well plates, or LNCaP ZBTB10-HA stable cells or LNCaP vector cells were plated in triplicate at 3000 cells/well in 96

well plates, one plate per irradiation condition, either in phenol-red free DMEM-F12 media containing 5% non-heat inactivated FBS and 1x ITS for enzalutamide condition or phenol-red free DMEM-F12 media containing 5% charcoal-stripped FBS and 1x ITS for the R1881 condition. Immediately following plating, 0.05 nM R1881 was added to cells designated to receive hormone stimulation. 24 hours after plating and 30 minutes prior to irradiation, 10 μM enzalutamide was added to cells designated to receive the inhibitor. The cells were treated with 0, 2, 6 Gy of radiation. CyQuant Direct reagent was added on day 6 according to the manufacturer's protocol (ThermoFisher). Quantification was performed using a BioTek Synergy 2 plate reader.

References

1. Rawla P. Epidemiology of Prostate Cancer. World J Oncol. 2019;10:63–89.

2. Wang G, Zhao D, Spring DJ, DePinho RA. Genetics and biology of prostate cancer. Genes Dev. 2018;32:1105–40.

3. Pozas J, Álvarez Rodríguez S, Fernández VA, Burgos J, Santoni M, Manneh Kopp R, et al. Androgen Receptor Signaling Inhibition in Advanced Castration Resistance Prostate Cancer: What Is Expected for the Near Future? Cancers (Basel). 2022;14:6071.

4. Attard G, Parker C, Eeles RA, Schröder F, Tomlins SA, Tannock I, et al. Prostate cancer. Lancet. 2016;387:70–82.

5. Ta HQ, Gioeli D. The convergence of DNA damage checkpoint pathways and androgen receptor signaling in prostate cancer. Endocr Relat Cancer. 2014;

6. Schiewer MJ, Knudsen KE. DNA Damage Response in Prostate Cancer. Cold Spring Harb Perspect Med. 2019;9.

7. Goodwin JF, Schiewer MJ, Dean JL, Schrecengost RS, de Leeuw R, Han S, et al. A hormone-DNA repair circuit governs the response to genotoxic insult. Cancer Discov. 2013;3:1254–71.

8. Polkinghorn WR, Parker JS, Lee MX, Kass EM, Spratt DE, Iaquinta PJ, et al. Androgen receptor signaling regulates DNA repair in prostate cancers. Cancer Discov. 2013;3:1245–53.

9. Bartek J, Mistrik M, Bartkova J. Androgen Receptor Signaling Fuels DNA Repair and Radioresistance in Prostate Cancer. Cancer Discovery. 2013;3:1222–4.

10. Jividen K, Kedzierska KZ, Yang C-S, Szlachta K, Ratan A, Paschal BM. Genomic analysis of DNA repair genes and androgen signaling in prostate cancer. BMC Cancer. 2018;18:960.

11. Li L, Karanika S, Yang G, Wang J, Park S, Broom BM, et al. Androgen receptor inhibitor-induced "BRCAness" and PARP inhibition are synthetically lethal for castration-resistant prostate cancer. Sci Signal. 2017;10.

12. Schiewer MJ, Goodwin JF, Han S, Brenner JC, Augello MA, Dean JL, et al. Dual roles of PARP-1 promote cancer growth and progression. Cancer Discov. 2012;2:1134–49.

13. Mayeur GL, Kung WJ, Martinez A, Izumiya C, Chen DJ, Kung HJ. Ku is a novel transcriptional recycling coactivator of the androgen receptor in prostate cancer cells. J Biol Chem. 2005;280:10827–33.

14. Yeh S, Hu YC, Rahman M, Lin HK, Hsu CL, Ting HJ, et al. Increase of androgen-induced cell death and androgen receptor transactivation by BRCA1 in prostate cancer cells. Proc Natl Acad Sci USA. 2000;97:11256–61.

15. Wang L, Hsu C-L, Ni J, Wang P-H, Yeh S, Keng P, et al. Human checkpoint protein hRad9 functions as a negative coregulator to repress androgen receptor transactivation in prostate cancer cells. Mol Cell Biol. 2004;24:2202–13.

16. Wang C, Sun H, Zou R, Zhou T, Wang S, Sun S, et al. MDC1 functionally identified as an androgen receptor co-activator participates in suppression of prostate cancer. Nucleic Acids Res. 2015;43:4893–908.

17. Yin Y, Li R, Xu K, Ding S, Li J, Baek G, et al. Androgen Receptor Variants Mediate DNA Repair after Prostate Cancer Irradiation. Cancer Res. 2017;77:4745–54.

18. Ta HQ, Ivey ML, Frierson HF, Conaway MR, Dziegielewski J, Larner JM, et al. Checkpoint Kinase 2 Negatively Regulates Androgen Sensitivity and Prostate Cancer Cell Growth. Cancer Res. 2015;75:5093–105.

19. Ta HQ, Dworak N, Ivey ML, Roller DG, Gioeli D. AR phosphorylation and CHK2 kinase activity regulates IR-stabilized AR-CHK2 interaction and prostate cancer survival. Elife. 2020;9:e51378.

20. Liberzon A, Birger C, Thorvaldsdóttir H, Ghandi M, Mesirov JP, Tamayo P. The Molecular Signatures Database (MSigDB) hallmark gene set collection. Cell Syst. 2015;1:417–25.

21. Wang Z, Chu T, Choate LA, Danko CG. Identification of regulatory elements from nascent transcription using dREG. Genome Res. 2019;29:293–303.

22. Bailey TL, Elkan C. Fitting a mixture model by expectation maximization to discover motifs in biopolymers. Proc Int Conf Intell Syst Mol Biol. 1994;2:28–36.

23. Castro-Mondragon JA, Riudavets-Puig R, Rauluseviciute I, Berhanu Lemma R, Turchi L, Blanc-Mathieu R, et al. JASPAR 2022: the 9th release of the open-access database of transcription factor binding profiles. Nucleic Acids Research. 2022;50:D165–73.

24. Grant CE, Bailey TL, Noble WS. FIMO: scanning for occurrences of a given motif. Bioinformatics. 2011;27:1017–8.

25. Cato L, Neeb A, Sharp A, Buzón V, Ficarro SB, Yang L, et al. Development of Bag-1L as a therapeutic target in androgen receptor-dependent prostate cancer. Elife. 2017;6.

26. R Z, C W, S M, Q Q, Q W, H S, et al. Cistrome Data Browser: expanded datasets and new tools for gene regulatory analysis. Nucleic acids research [Internet]. Nucleic Acids Res; 2019 [cited 2023 Feb 22];47. Available from: https://pubmed.ncbi.nlm.nih.gov/30462313/

27. Toropainen S, Niskanen EA, Malinen M, Sutinen P, Kaikkonen MU, Palvimo JJ. Global analysis of transcription in castration-resistant prostate cancer cells uncovers active enhancers and direct androgen receptor targets. Sci Rep. 2016;6:33510.

28. Malinen M, Niskanen EA, Kaikkonen MU, Palvimo JJ. Crosstalk between androgen and pro-inflammatory signaling remodels androgen receptor and NF-κB cistrome to reprogram the prostate cancer cell transcriptome. Nucleic Acids Res. 2016;

29. Gioeli D, Ficarro SB, Kwiek JJ, Aaronson D, Hancock M, Catling AD, et al. Androgen receptor phosphorylation. Regulation and identification of the phosphorylation sites. J Biol Chem. 2002;277:29304–14.

30. Gordon V, Bhadel S, Wunderlich W, Zhang J, Ficarro SB, Mollah SA, et al. CDK9 regulates AR promoter selectivity and cell growth through serine 81 phosphorylation. Mol Endocrinol. 2010;24:2267–80.

31. Koryakina Y, Ta HQ, Gioeli D. Androgen receptor phosphorylation: biological context and functional consequences. Endocr Relat Cancer. 2014;21:T131-145.

32. Liu X, Kraus WL, Bai X. Ready, pause, go: regulation of RNA polymerase II pausing and release by cellular signaling pathways. Trends Biochem Sci. 2015;40:516–25.

33. Core L, Adelman K. Promoter-proximal pausing of RNA polymerase II: a nexus of gene regulation. Genes Dev. 2019;33:960–82.

34. Mahat DB, Kwak H, Booth GT, Jonkers IH, Danko CG, Patel RK, et al. Base-pair-resolution genome-wide mapping of active RNA polymerases using precision nuclear run-on (PRO-seq). Nat Protoc. 2016;11:1455–76.

35. Dutta AB, Lank DS, Przanowska RK, Przanowski P, Wang L, Nguyen B, et al. Kinetic networks identify TWIST2 as a key regulatory node in adipogenesis. Genome Res. 2023;33:314–31.

36. Tang Z, Kang B, Li C, Chen T, Zhang Z. GEPIA2: an enhanced web server for large-scale expression profiling and interactive analysis. Nucleic Acids Research. 2019;47:W556–60.

37. Uhlén M, Fagerberg L, Hallström BM, Lindskog C, Oksvold P, Mardinoglu A, et al. Proteomics. Tissue-based map of the human proteome. Science. 2015;347:1260419.

38. Lin C, Blessing AM, Pulliam TL, Shi Y, Wilkenfeld SR, Han JJ, et al. Inhibition of CAMKK2 impairs autophagy and castration-resistant prostate cancer via suppression of AMPK-ULK1 signaling. Oncogene. 2021;40:1690–705.

39. Penfold L, Woods A, Muckett P, Nikitin AY, Kent TR, Zhang S, et al. CAMKK2 Promotes Prostate Cancer Independently of AMPK via Increased Lipogenesis. Cancer Res. 2018;78:6747–61.

40. Tamura K, Makino A, Hullin-Matsuda F, Kobayashi T, Furihata M, Chung S, et al. Novel lipogenic enzyme ELOVL7 is involved in prostate cancer growth through saturated long-chain fatty acid metabolism. Cancer Res. 2009;69:8133–40.

41. Zheng D, Decker KF, Zhou T, Chen J, Qi Z, Jacobs K, et al. Role of WNT7B-induced noncanonical pathway in advanced prostate cancer. Mol Cancer Res. 2013;11:482–93.

42. Pulliam TL, Goli P, Awad D, Lin C, Wilkenfeld SR, Frigo DE. Regulation and role of CAMKK2 in prostate cancer. Nat Rev Urol. 2022;19:367–80.

43. Horwitz EM, Bae K, Hanks GE, Porter A, Grignon DJ, Brereton HD, et al. Ten-year follow-up of radiation therapy oncology group protocol 92-02: a phase III trial of the duration of elective androgen deprivation in locally advanced prostate cancer. J Clin Oncol. 2008;26:2497–504.

44. Bolla M, Collette L, Blank L, Warde P, Dubois JB, Mirimanoff R-O, et al. Long-term results with immediate androgen suppression and external irradiation in patients with locally advanced prostate cancer (an EORTC study): a phase III randomised trial. Lancet. 2002;360:103–6.

45. Pilepich MV, Winter K, John MJ, Mesic JB, Sause W, Rubin P, et al. Phase III radiation therapy oncology group (RTOG) trial 86-10 of androgen deprivation adjuvant to definitive radiotherapy in locally advanced carcinoma of the prostate. Int J Radiat Oncol Biol Phys. 2001;50:1243–52.

46. Pilepich MV, Winter K, Lawton CA, Krisch RE, Wolkov HB, Movsas B, et al. Androgen suppression adjuvant to definitive radiotherapy in prostate carcinoma--long-term results of phase III RTOG 85-31. Int J Radiat Oncol Biol Phys. 2005;61:1285–90.

47. Kishan AU, Sun Y, Hartman H, Pisansky TM, Bolla M, Neven A, et al. Androgen deprivation therapy use and duration with definitive radiotherapy for localised prostate cancer: an individual patient data meta-analysis. The Lancet Oncology. 2022;23:304–16.

48. Campbell PJ, Getz G, Korbel JO, Stuart JM, Jennings JL, Stein LD, et al. Pan-cancer analysis of whole genomes. Nature. Nature Publishing Group; 2020;578:82–93.

49. Abida W, Cyrta J, Heller G, Prandi D, Armenia J, Coleman I, et al. Genomic correlates of clinical outcome in advanced prostate cancer. Proc Natl Acad Sci USA. 2019;116:11428–36.

50. Tomlins SA, Laxman B, Varambally S, Cao X, Yu J, Helgeson BE, et al. Role of the TMPRSS2-ERG Gene Fusion in Prostate Cancer. Neoplasia. 2008;10:177–88.

51. Sun C, Dobi A, Mohamed A, Li H, Thangapazham RL, Furusato B, et al. TMPRSS2-ERG fusion, a common genomic alteration in prostate cancer activates C-MYC and abrogates prostate epithelial differentiation. Oncogene. 2008;27:5348–53.

52. Barfeld SJ, Urbanucci A, Itkonen HM, Fazli L, Hicks JL, Thiede B, et al. c-Myc Antagonises the Transcriptional Activity of the Androgen Receptor in Prostate Cancer Affecting Key Gene Networks. EBioMedicine. 2017;18:83–93.

53. Guo H, Wu Y, Nouri M, Spisak S, Russo JW, Sowalsky AG, et al. Androgen receptor and MYC equilibration centralizes on developmental super-enhancer. Nat Commun. 2021;12:7308.

54. Qiu X, Boufaied N, Hallal T, Feit A, de Polo A, Luoma AM, et al. MYC drives aggressive prostate cancer by disrupting transcriptional pause release at androgen receptor targets. Nat Commun. Nature Publishing Group; 2022;13:2559.

55. Fujinaga K, Huang F, Peterlin BM. P-TEFb: The master regulator of transcription elongation. Mol Cell. 2023;83:393–403.

56. Chen S, Xu Y, Yuan X, Bubley GJ, Balk SP. Androgen receptor phosphorylation and stabilization in prostate cancer by cyclin-dependent kinase 1. Proc Natl Acad Sci U S A [Internet]. 2006; Available from: http://www.ncbi.nlm.nih.gov/entrez/query.fcgi?cmd=Retrieve&db=PubMed&dopt=Citation&list_uids=17043241

57. Chen S, Gulla S, Cai C, Balk SP. Androgen receptor serine 81 phosphorylation mediates chromatin binding and transcriptional activation. J Biol Chem. 2012;287:8571–83.

58. Liu X, Gao Y, Ye H, Gerrin S, Ma F, Wu Y, et al. Positive feedback loop mediated by protein phosphatase 1α mobilization of P-TEFb and basal CDK1 drives androgen receptor in prostate cancer. Nucleic Acids Res. 2017;

59. Spratt DE, Malone S, Roy S, Grimes S, Eapen L, Morgan SC, et al. Prostate Radiotherapy With Adjuvant Androgen Deprivation Therapy (ADT) Improves Metastasis-Free Survival Compared to Neoadjuvant ADT: An Individual Patient Meta-Analysis. JCO. Wolters Kluwer; 2021;39:136–44.

60. Guan X, Polesso F, Wang C, Sehrawat A, Hawkins RM, Murray SE, et al. Androgen receptor activity in T cells limits checkpoint blockade efficacy. Nature. Nature Publishing Group; 2022;606:791–6.

61. Zhang X, Cheng L, Gao C, Chen J, Liao S, Zheng Y, et al. Androgen Signaling Contributes to Sex Differences in Cancer by Inhibiting NF-κB Activation in T Cells and Suppressing Antitumor Immunity. Cancer Res. 2023;83:906–21.

62. Ishihara D, Pop L, Takeshima T, Iyengar P, Hannan R. Rationale and evidence to combine radiation therapy and immunotherapy for cancer treatment. Cancer Immunol Immunother. 2017;66:281–98.

63. Mole RH. Whole Body Irradiation—Radiobiology or Medicine? BJR. The British Institute of Radiology; 1953;26:234–41.

64. Sathyan KM, McKenna BD, Anderson WD, Duarte FM, Core L, Guertin MJ. An improved auxin-inducible degron system preserves native protein levels and enables rapid and specific protein depletion. Genes Dev. 2019;33:1441–55.

65. Dutta AB, Lank DS, Przanowska RK, Przanowski P, Wang L, Nguyen B, et al. Kinetic networks identify Twist2 as a key regulatory node in adipogenesis [Internet]. bioRxiv; 2022 [cited 2023 Feb 22]. page 2021.11.17.469040. Available from: https://www.biorxiv.org/content/10.1101/2021.11.17.469040v2

66. Scott TG, Martins AL, Guertin MJ. Processing and evaluating the quality of genome-wide nascent transcription profiling libraries [Internet]. bioRxiv; 2022 [cited 2023 Feb 22]. page 2022.12.14.520463. Available from: https://www.biorxiv.org/content/10.1101/2022.12.14.520463v1

67. Gordon V, Bhadel S, Wunderlich W, Zhang J, Ficarro SB, Mollah SA, et al. CDK9 regulates AR promoter selectivity and cell growth through serine 81 phosphorylation. Molecular Endocrinology (Baltimore, Md). 2010;24:2267–80.

68. Whitworth H, Bhadel S, Ivey M, Conaway M, Spencer A, Hernan R, et al. Identification of Kinases Regulating Prostate Cancer Cell Growth Using an RNAi Phenotypic Screen. PLoS ONE. 2012;7.

69. Wong ML, Medrano JF. Real-time PCR for mRNA quantitation. BioTechniques. 2005;39:75–85.

70. Bustin SA. Absolute quantification of mRNA using real-time reverse transcription polymerase chain reaction assays. J Mol Endocrinol. 2000;25:169–93.

71. Gordon MA, D'Amato NC, Gu H, Babbs B, Wulfkuhle JD, Petricoin EF, et al. Synergy between androgen receptor antagonism and inhibition of mTOR and HER2 in breast cancer. Mol Cancer Ther. 2017;

72. Whitworth H, Bhadel S, Ivey M, Conaway M, Spencer A, Hernan R, et al. Identification of Kinases Regulating Prostate Cancer Cell Growth Using an RNAi Phenotypic Screen. PLoS ONE. 2012;7:e38950.

Figure 1. IR activates a p53 transcriptional response in PCa cells. (A) Outline of experiment. (B) Principal Component analysis of PRO-seq for control or radiation (6Gy) samples. (C) Heat map of PRO-seq signal reflecting gene expression values, scaled by row. (D) Volcano plot highlighting differentially expressed genes upon radiation treatment. The horizontal dashed black line denotes an adjusted p-value of 0.1. Points having a positive or negative fold-change are shown in red (up in response to radiation) or blue (down in response to radiation), respectively. (E) GSEA of IR-induced primary transcriptional response (FDR 0.05). (F) *de novo* identified motif from IR-activated putative regulatory elements matching the canonical p53 motif from the JASPAR database. (G) Differential p53 motif prevalence in putative regulatory elements that change in response to radiation.

Figure 2. The directly AR-regulated transcriptome is not a major contributor to the immediate transcriptional response to DNA damage. (A) Outline of experiment. (B) Validation of growth inhibition by AR antagonism in LNCaP cells. (C) Validation of radiosensitization with AR antagonism using 10µM enzalutamide and radioprotection with AR activation using 0.05nM R1881. (D) Principal Component analysis of PRO-seq for control, radiation (6Gy), enzalutamide (10µM), and radiation+enzalutamide (6Gy+10µM enzalutamide) samples. (E) Heat map of PRO-seq signal reflecting gene expression values, scaled by row. (F) Volcano plot highlighting differentially expressed genes upon radiation treatment (left) or enzalutamide treatment (right). (G) Volcano plot highlighting differentially expressed genes in the Hallmark DNA Repair gene set upon radiation treatment (left) or enzalutamide treatment (right). (H) Volcano plot highlighting differentially expressed genes in our primary AR target gene set upon enzalutamide

treatment (left) or radiation treatment (right). (I) Volcano plot highlighting differentially expressed genes in the Hallmark DNA Repair gene set upon radiation treatment. In (F-I), the horizontal dashed black line denotes an adjusted p-value of 0.1. Points having a positive or negative fold-change are shown in red (up in response to radiation or enzalutamide) or blue (down in response to radiation or enzalutamide), respectively. (J-L) Cumulative Distribution Function plots of the distances from the TSS of (J) IR-activated genes to AR binding sites, (K) enzalutamide-repressed genes to AR binding sites, and (L) IR-activated genes to p53 binding sites.

Figure 3. Enzalutamide treatment prevents Pol II promoter-proximal pause release triggered by IR within a subset of genes. (A) Pol II density plot of radiation-activated genes in radiation and control conditions. (B) Box and whisker and violin plot of the log-transformed ratio of pause index (PI) for radiation-activated genes in radiation and control conditions. (C) Pol II density plot of enzalutamide-repressed genes in enzalutamide and vehicle conditions. (D) Box and whisker and violin plot of the log-transformed ratio of PI for enzalutamide-repressed genes in enzalutamide and vehicle conditions. (E) Normalized count expression data for genes activated by radiation and repressed by enzalutamide. (F) Box and whisker and violin plot of the log-transformed ratio of PI for the 16 genes in (E) for the different treatments relative to the control and vehicle condition.

Figure 4. Regulation of candidate AR-regulated DDR genes in PCa tumors and LNCaP cells. (A) GEPIA2 analysis of the PCa TCGA and GTEx data of the top eight genes; * <0.01. (B) Normalized

mRNA expression of CAMKK2, CDC42EP3, ELOVL7, PMEPA1, PVT1, TLE1, and WNT7B at 24hrs in response to 6Gy radiation, 10µM enzalutamide, or combination thereof. * <0.05, ** <0.005, **** <0.0001 indicating a statistically significant effect of enzalutamide on control or IR, using ANOVA followed by Sidak's multiple comparisons test. (C) Western blot data of ELOVL7, and loading controls Tubulin and Ran, over time (15 minutes, 1 hour, 4 hours, and 6 hours) in response to 6Gy radiation (IR), 10µM enzalutamide (E), or combination thereof (E+IR), and control (C) vehicle treated cells. (D) Quantitation of ELOVL7 expression normalized to Tubulin and Ran, with control at 15 minutes set to zero, n= 3 to 4.

Figure 5. Effect of ZBTB10 overexpression on IR cell survival. (A) Log-transformed fold change and adjusted p-values of TFs repressed by enzalutamide. (B) Disease-free survival plot from the PCa TCGA showing a worse prognosis associated with alterations with ZBTB10 (q=0.041). (C) GEPIA2 analysis of the PCa TCGA and GTEx data of ZBTB10; *p<0.05. (D) LNCaP (E) C4-2, Rv1, VCaP normalized mRNA expression of ZBTB10 at 24 hours in response to 6Gy radiation, 10µM enzalutamide, or combination thereof. * <0.05, ** <0.005, *** <0.0005, **** <0.0001, using ANOVA followed by Sidak's multiple comparisons test. (F, G) Relative growth over seven days in LNCaP ZBTB10 overexpression cells were irradiated with 0, 2, 4, or 6Gy and treated with vehicle control or 10µM enzalutamide (F) or 0.05nM R1881 (G). (H, I) Validation of ZBTB10 overexpression showing mRNA (H) and protein (I) expression of LNCaP ZBTB10 stable mass population and vector control.

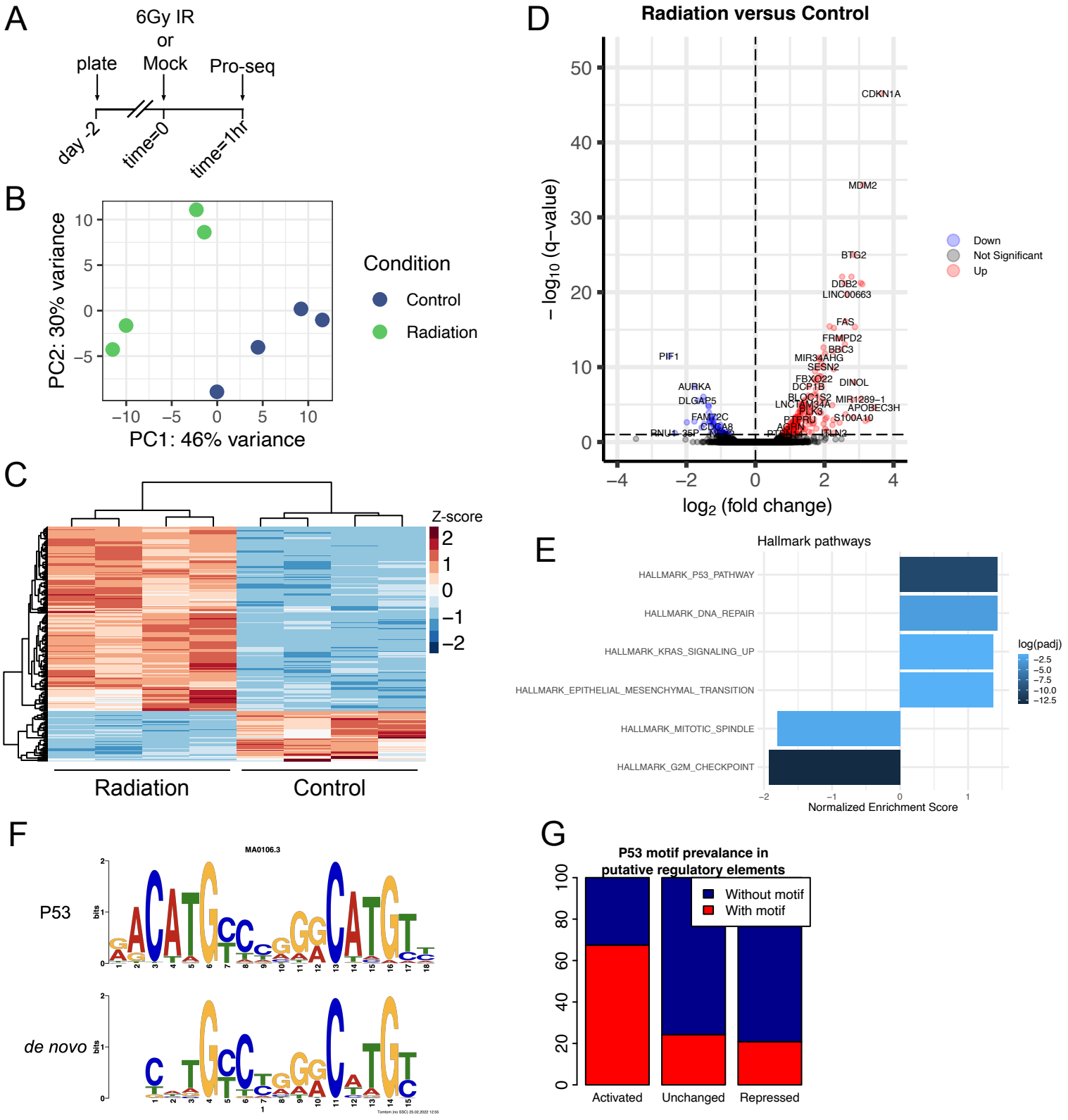
A
6Gy IR
or
Mock
plate
Pro-seq
day -2
time=0
time=1hr
B
PC2: 30% variance
PC1: 46% variance
Condition
Control
Radiation
C
Z-score
Radiation
Control
D
Radiation versus Control
− log10 (q−value)
log2 (fold change)
Down
Not Significant
Up
CDKN1A
MDM2
BTG2
DDB2
LINC00663
FAS
FRMPD2
BBC3
MIR34AHG
SESN2
DINOL
MIR1289−1
APOBEC3H
S100A10
PIF1
AURKA
DLGAP5
E
Hallmark pathways
HALLMARK_P53_PATHWAY
HALLMARK_DNA_REPAIR
HALLMARK_KRAS_SIGNALING_UP
HALLMARK_EPITHELIAL_MESENCHYMAL_TRANSITION
HALLMARK_MITOTIC_SPINDLE
HALLMARK_G2M_CHECKPOINT
Normalized Enrichment Score
log(padj)
F
MA0106.3
P53
de novo
G
P53 motif prevalance in
putative regulatory elements
Without motif
With motif
Activated
Unchanged
Repressed

Figure 1

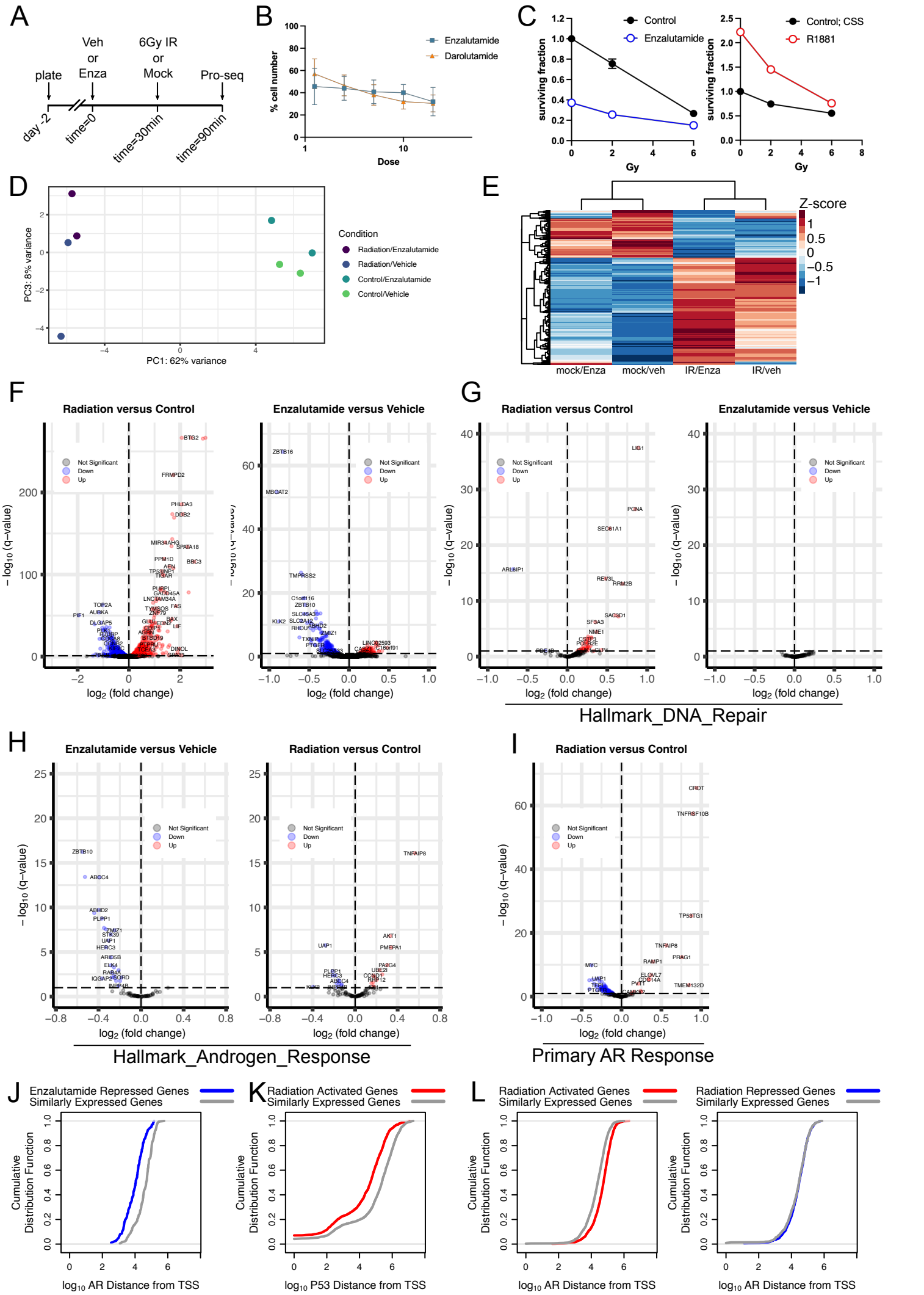
A
plate
Veh or Enza
6Gy IR or Mock
Pro-seq
day -2
time=0
time=30min
time=90min
B
% cell number
Dose
Enzalutamide
Darolutamide
C
surviving fraction
Gy
Control
Enzalutamide
Control; CSS
R1881
D
PC3: 8% variance
PC1: 62% variance
Condition
Radiation/Enzalutamide
Radiation/Vehicle
Control/Enzalutamide
Control/Vehicle
E
Z-score
mock/Enza
mock/veh
IR/Enza
IR/veh
F
Radiation versus Control
Enzalutamide versus Vehicle
Not Significant
Down
Up
– log10 (q–value)
log2 (fold change)
G
Radiation versus Control
Enzalutamide versus Vehicle
Hallmark_DNA_Repair
H
Enzalutamide versus Vehicle
Radiation versus Control
Hallmark_Androgen_Response
I
Radiation versus Control
Primary AR Response
J
Enzalutamide Repressed Genes
Similarly Expressed Genes
Cumulative Distribution Function
log10 AR Distance from TSS
K
Radiation Activated Genes
Similarly Expressed Genes
log10 P53 Distance from TSS
L
Radiation Activated Genes
Radiation Repressed Genes
Similarly Expressed Genes

Figure 2

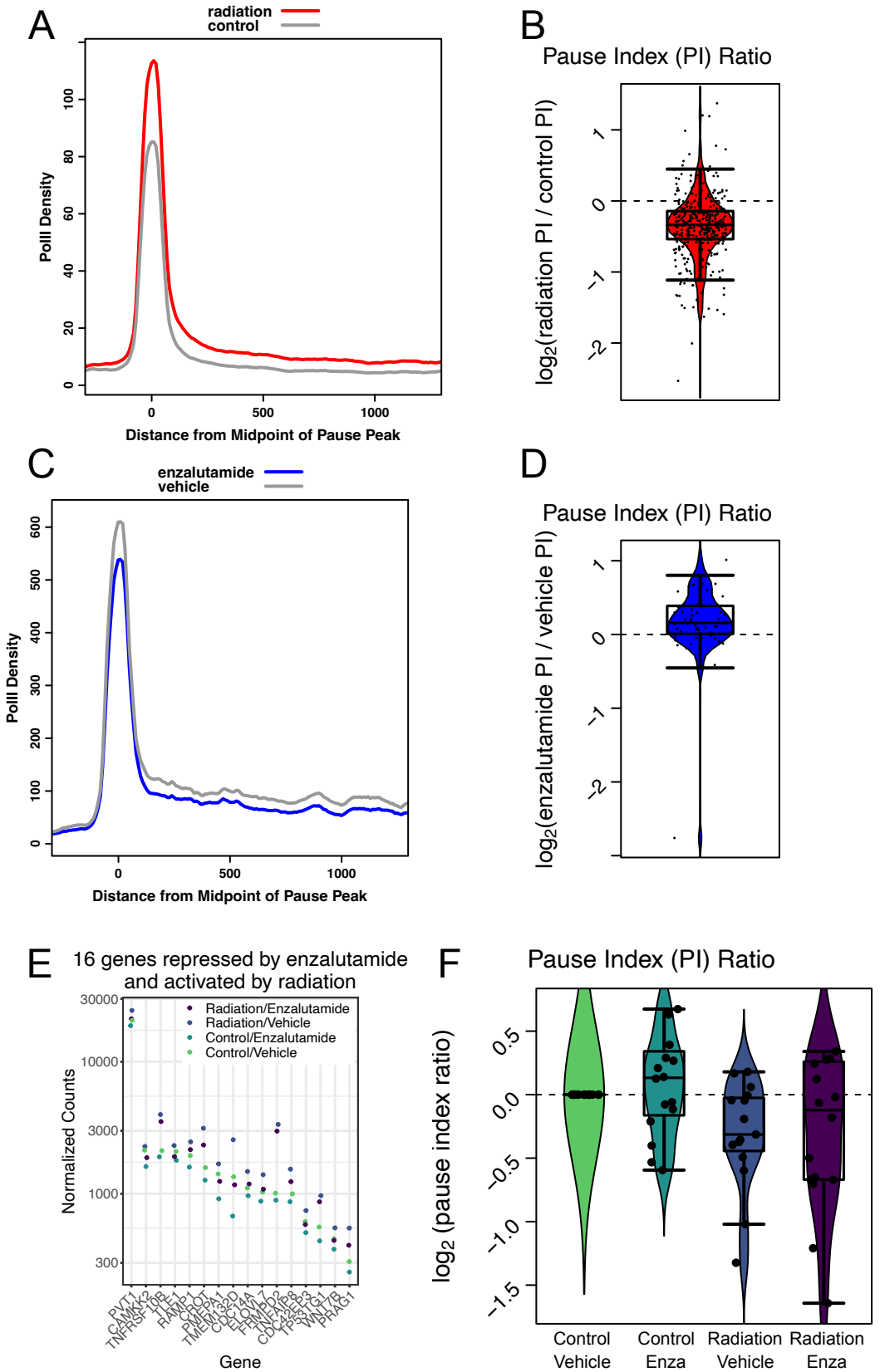
A
radiation
control
PolII Density
Distance from Midpoint of Pause Peak
B
Pause Index (PI) Ratio
log2(radiation PI / control PI)
C
enzalutamide
vehicle
PolII Density
Distance from Midpoint of Pause Peak
D
Pause Index (PI) Ratio
log2(enzalutamide PI / vehicle PI)
E
16 genes repressed by enzalutamide and activated by radiation
Radiation/Enzalutamide
Radiation/Vehicle
Control/Enzalutamide
Control/Vehicle
Normalized Counts
Gene
F
Pause Index (PI) Ratio
log2 (pause index ratio)
Control Vehicle
Control Enza
Radiation Vehicle
Radiation Enza

Figure 3

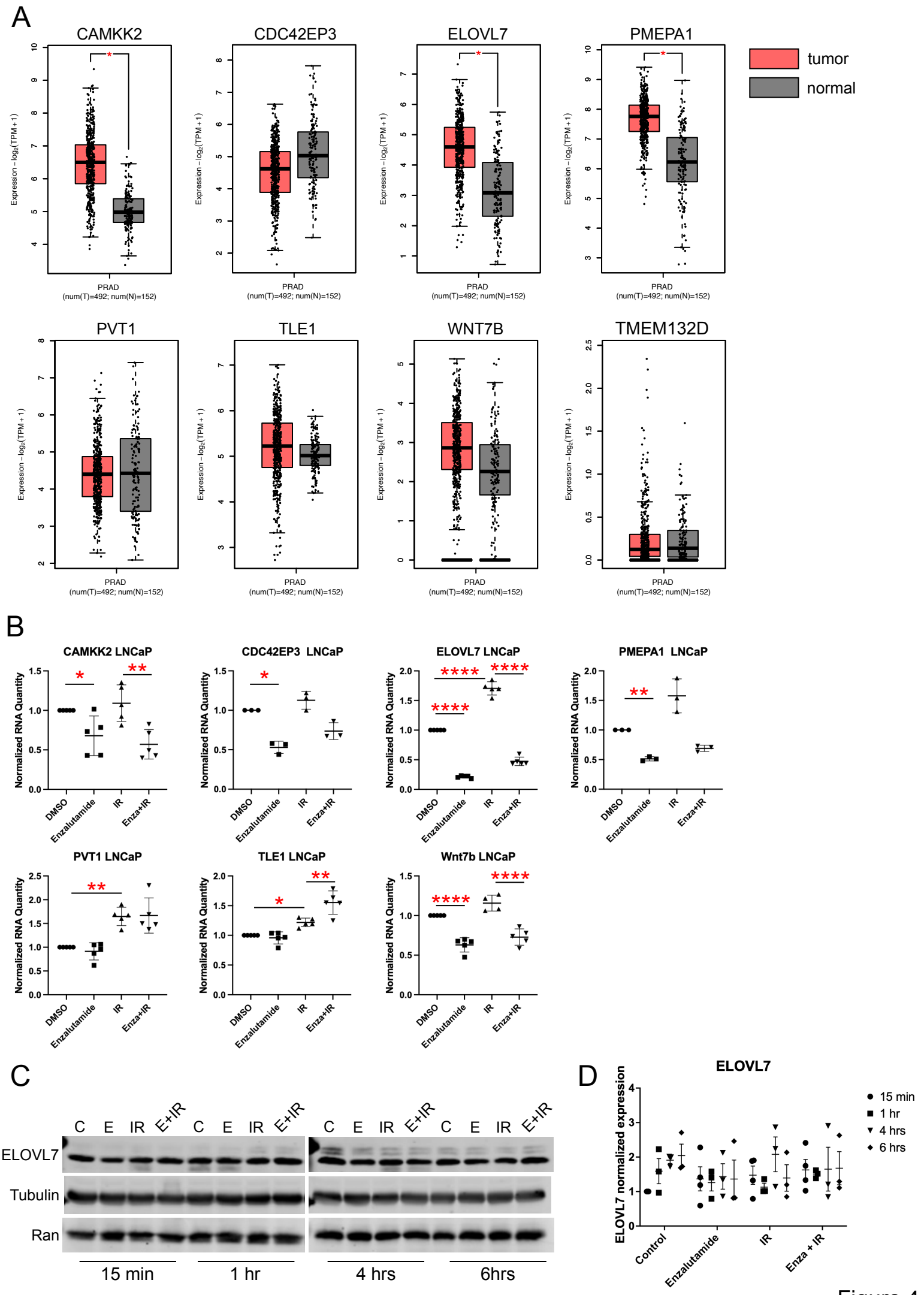
A
CAMKK2
CDC42EP3
ELOVL7
PMEPA1
tumor
normal
Expression – log2(TPM+1)
PRAD
(num(T)=492; num(N)=152)
PVT1
TLE1
WNT7B
TMEM132D
B
CAMKK2 LNCaP
CDC42EP3 LNCaP
ELOVL7 LNCaP
PMEPA1 LNCaP
PVT1 LNCaP
TLE1 LNCaP
Wnt7b LNCaP
Normalized RNA Quantity
DMSO
Enzalutamide
IR
Enza+IR
C
C E IR E+IR C E IR E+IR C E IR E+IR C E IR E+IR
ELOVL7
Tubulin
Ran
15 min
1 hr
4 hrs
6hrs
D
ELOVL7
ELOVL7 normalized expression
15 min
1 hr
4 hrs
6 hrs
Control
Enzalutamide
IR
Enza + IR

Figure 4

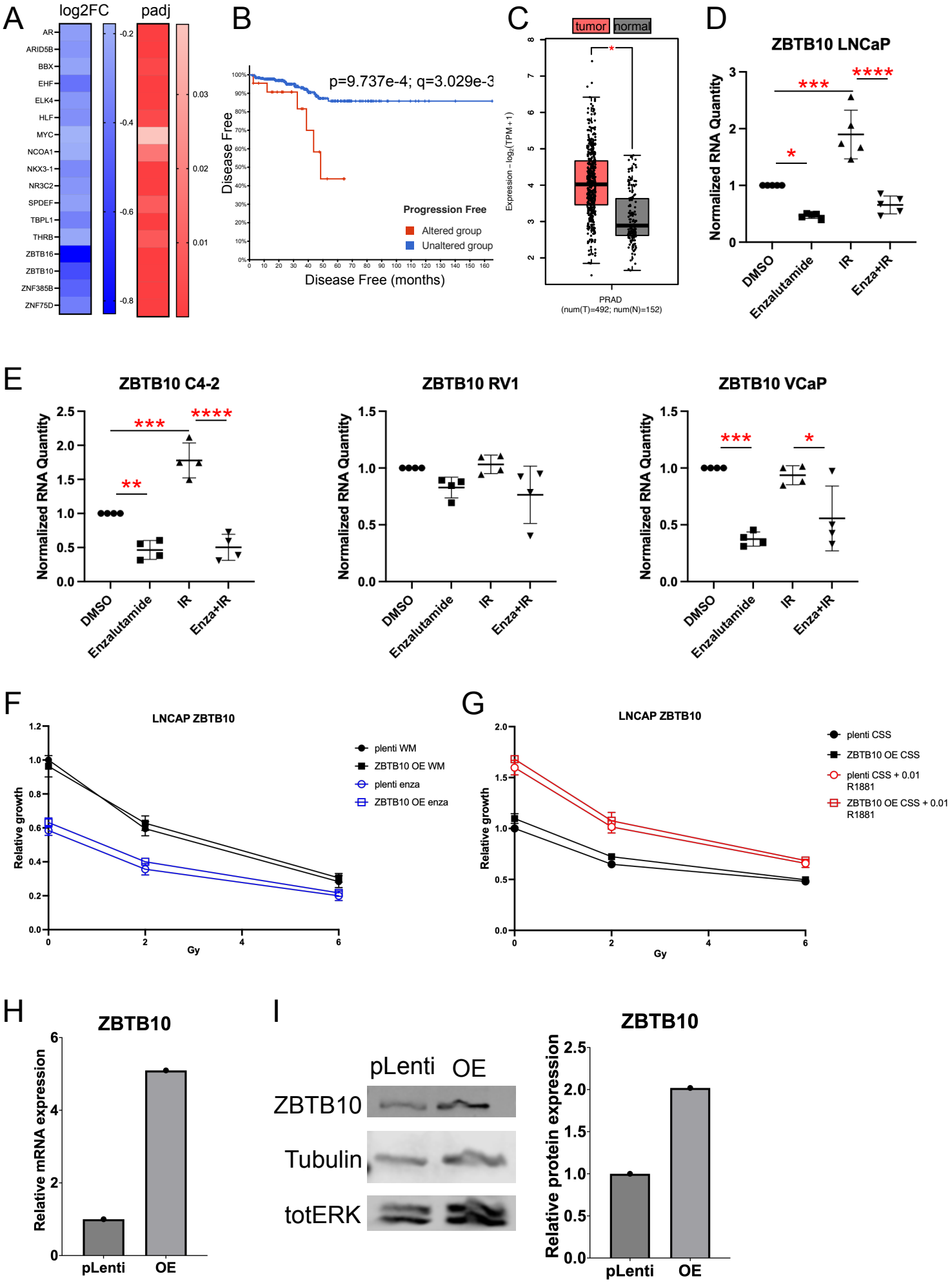
A
log2FC
padj
AR
ARID5B
BBX
EHF
ELK4
HLF
MYC
NCOA1
NKX3-1
NR3C2
SPDEF
TBPL1
THRB
ZBTB16
ZBTB10
ZNF385B
ZNF75D
B
p=9.737e-4; q=3.029e-3
Disease Free
Disease Free (months)
Progression Free
Altered group
Unaltered group
C
tumor
normal
PRAD
(num(T)=492; num(N)=152)
D
ZBTB10 LNCaP
Normalized RNA Quantity
DMSO
Enzalutamide
IR
Enza+IR
E
ZBTB10 C4-2
ZBTB10 RV1
ZBTB10 VCaP
F
LNCAP ZBTB10
Relative growth
Gy
plenti WM
ZBTB10 OE WM
plenti enza
ZBTB10 OE enza
G
LNCAP ZBTB10
plenti CSS
ZBTB10 OE CSS
plenti CSS + 0.01 R1881
ZBTB10 OE CSS + 0.01 R1881
H
ZBTB10
Relative mRNA expression
pLenti
OE
I
pLenti
OE
ZBTB10
Tubulin
totERK
ZBTB10
Relative protein expression

Figure 5